Effects of Cooling Rate and Solute Content on the Grain Refinement of Mg-Gd-Y Alloys by Aluminum

JICHUN DAI, MARK A. EASTON, MINGXING ZHANG, DONG QIU, XIANGYUAN XIONG, WENCAI LIU, and GUOHUA WU

The effect of Al additions on grain refinement of Mg-Gd-Y alloys with different solute contents at different cooling rates has been investigated. For all alloys, significant grain refinement was due to the formation of $Al_2(Gd_xY_{1-x})$ nucleant particles. The number density and size distribution of $Al_2(Gd_xY_{1-x})$ were affected by both solute content and the cooling rate. Grain sizes (d_{gs}) of Mg-Gd-Y base alloys and of Mg-Gd-Y-Al alloys were related to solute content (defined by the growth restriction factor, Q), cooling rate ($\dot{T}$), and area number density (ρ_{ns}) and size (d_p) of nucleant particles that can be activated. It is found that grain sizes of Mg-Gd-Y base alloys follow the relationship $d_{gs} = a + \frac{b}{Q\sqrt{\dot{T}}}$, while grain sizes of Al-refined samples follow the relationship $d_{gs} = \frac{a'}{\sqrt{\rho_{ns}}} + \frac{b'}{\sqrt{\dot{T}Qd_p}}$, where a, b, a', and b' were constants. In addition, the grain refinement effect of Al additions was more susceptible to solute content and the cooling rate than that of Zr which is regarded as the most efficient grain refiner for Mg alloys.

DOI: 10.1007/s11661-014-2390-2

I. INTRODUCTION

GRAIN refinement is beneficial to cast components by producing a uniform distribution of secondary phases, improved castability and mechanical properties.[1] The formation of grains consists of two steps: nucleation and subsequent growth. Enhancing the nucleation rate and/or reducing the growth rate of grains refine the grains.[2] Hence, nucleants and/or solute are usually added into melts to refine grains. On the one hand, nucleant particles promote primary heterogeneous nucleation during solidification due to small undercooling required.[3] Both the interfacial energy and size of nucleant particles are important in grain refinement.[4–8] On the other hand, solute atoms that segregate in front of the solid–liquid interface provide constitutional supercooling (CS), which reduces the velocity of grain growth and facilitates subsequent nucleation provided that further nucleant substrates are available in the CS zone.[2,3,9] Both experimental observations and theoretical analysis indicate that the growth restriction factor, Q, is an adequate parameter to measure the effect of solute on grain refinement of aluminum and magnesium alloys, and the grain size always has an approximately linear relationship with the reciprocal of Q.[2,9–11] Further details about Q will be provided in Section A of the Discussion. Other than nucleants and solute, solidification conditions also significantly affect the grain size of cast components.[12–15] Moreover, the solidification conditions can also affect the morphology of intermetallic particles.[16,17]

Magnesium alloys containing rare earth (RE) elements usually exhibit excellent mechanical properties.[18] Among them, Mg-Gd-Y base alloys are promising because they possess higher strength and creep resistance than WE54 (Mg-5Y-4RE, all compositions are in weight percentage throughout this article unless specified), the prevailing high-strength commercial Mg alloy.[19–21] Recent research found that Mg-10Y,[22] Mg-10Gd,[23] and Mg-10Gd-3Y[24] alloys can be significantly grain refined by the addition of Al due to the formation of Al_2RE nucleant particles, *i.e.*, Al_2Y, Al_2Gd, and $Al_2(Gd_{0.5}Y_{0.5})$ prior to the solidification of α-Mg. Based upon the introduction in the above paragraph, it would be expected that the grain size of the Al_2RE-refined alloys would be affected by solute content and cooling condition. Furthermore, the size and number density of Al_2RE nucleant particles should also subject to the solute content and cooling condition, which would subsequently influence the refined grain size.[5] However, no experimental work has been

JICHUN DAI, Ph.D. Student, is with the National Engineering Research Center of Light Alloy Net Forming, Shanghai Jiao Tong University, Shanghai 200240, P.R. China, and also with the School of Aerospace, Mechanical and Manufacturing Engineering, RMIT University, Bundoora VIC 3083, Australia. MARK A. EASTON, Professor, is with the School of Aerospace, Mechanical and Manufacturing Engineering, RMIT University. MINGXING ZHANG, Professor, and DONG QIU, Research Fellow, are with the Division of Materials, School of Mechanical and Mining Engineering, The University of Queensland, St Lucia, Brisbane, QLD 4072, Australia. XIANGYUAN XIONG, Senior Lecturer, is with the Department of Materials Engineering, Monash University, Clayton, VIC 3800, Australia. WENCAI LIU, Assistant Researcher, is with the National Engineering Research Center of Light Alloy Net Forming, Shanghai Jiao Tong University. GUOHUA WU, Professor, is with the National Engineering Research Center of Light Alloy Net Forming and also with the State Key Laboratory of Metal Matrix Composites, Shanghai Jiao Tong University, Shanghai 200240, P.R. China. Contact e-mail: ghwu@sjtu.edu.cn
Manuscript submitted November 20, 2013.
Article published online July 2, 2014

reported yet in terms of the effect of solute content and cooling condition on grain refining efficiency of Al_2RE particles when Al additions are used to refine grains.

In the present work, the grain refinement behavior of Mg-Gd-Y alloys with different Gd and Y contents through Al inoculation at four cooling rates was comprehensively investigated. The effects of solute content and cooling rate on the size distribution and number density of Al_2RE particles were also studied. The relationship between grain size and some key parameters, *i.e.*, solute content, cooling rate, and number density and size of nucleant particles was analyzed and discussed based on earlier research.[2,9,12,25]

II. EXPERIMENTAL PROCEDURE

Four Mg-Gd-Y alloys (Mg-3Gd-0.6Y, Mg-5Gd-1Y, Mg-7Gd-1.4Y, and Mg-10Gd-2Y) were made from pure Mg, Mg-90 pct Gd, and Mg-30 pct Y master alloys in an electric furnace under a mixed protective atmosphere of AM-COVER gas.[26] Pure Al was added into the melt whilst maintaining the melt temperature at 1013 K (740 °C). The melt was stirred for 2 minutes, and then held at 1013 K (740 °C) for 30 minutes to allow Gd, Y, and Al to fully dissolve before samples were taken. A dry mild steel cone ladle coated with BN (Ø 30 × Ø 20 × 25 mm) was preheated on the top of the melt for 1 minute to the same temperature as the melt, and then the ladle was filled with the melt at the top of the furnace crucible and solidified at four different cooling rates in the range from 1.4 to 22.6 K/s similar to the technique developed by Backerud *et al.*[27] which has been used by other researchers.[12,15] The advantage of this method is that the formation of wall crystals is minimized or even eliminated through using preheated ladles.

A presolidification cooling rate of 1.4 K/s was obtained by packing Fibrefrax® on the bottom and sides of the ladle. To obtain a cooling rate of 3.0 K/s, the ladle was allowed to cool in air. A cooling rate of 16.5 K/s was obtained by putting the ladle into a low-melting point alloy, *i.e.*, a 633 K (360 °C) Bi-Sn melt. A higher cooling rate of 22.6 K/s was obtained by putting the sample into a 433 K (160 °C) Bi-Sn melt. Under each cooling condition, the cooling rate was measured by K-type thermocouples placed in the center 10 mm from the bottom of the ladle. The actual compositions of the alloys were measured by an Optima 7300DV inductively coupled plasma atomic emission spectroscopy (ICP-AES) (PerkinElmer Inc., Waltham, MA) and are listed in Table I.

All metallographic samples were cut along the radial direction at 10 mm from the bottom of ingots, mechanically polished, etched in an acetic-picric solution (10 mL acetic acid, 6 g picric acid and 8 mL H_2O in 70 mL ethanol) and then examined using an OLYMPUS optical microscope under polarized light in order to measure the average grain size. The average grain size was measured by a linear intercept method according to ASTM 112-96. Microstructures were further examined using a JEOL JSM-7001F field emission scanning electron microscope (SEM) (Japan Electron Optics Ltd., Tokyo, Japan) equipped with energy-dispersive X-ray (EDX) spectrometry to reveal the microstructures of alloys and compositions of phases. The number density and size distribution of total $Al_2(Gd_xY_{1-x})$ particles (all particles at both grain centers and grain boundaries) and of possible active $Al_2(Gd_xY_{1-x})$ nucleant particles (only particles at grain centers) were calculated in 20–50 rectangular areas close to the center of the transverse section. In each sample, the area number density of particles, *i.e.*, the number of particles per unit area, was determined by dividing the total number of these particles in all fields by the total area of the fields of view. The size distribution of particles was obtained through *ex situ* measurement using Image-Pro Plus software.

Table I. Chemical Compositions of the Studied Alloys in this Work Determined by ICP-AES

	Elemental Composition (Wt Pct)			
Alloy	Gd	Y	Al	Mg
Mg-3Gd-0.6Y	2.74	0.80	—	bal.
Mg-3Gd-0.6Y-1Al	2.66	0.54	1.13	bal.
Mg-3Gd-0.6Y-2Al	2.84	0.51	2.43	bal.
Mg-5Gd-1Y	4.61	0.86	—	bal.
Mg-5Gd-1Y-1Al	4.37	0.62	1.28	bal.
Mg-7Gd-1.4Y	7.05	1.76	—	bal.
Mg-7Gd-1.4Y-1Al	7.29	1.10	1.27	bal.
Mg-10Gd-2Y	10.50	2.16	—	bal.
Mg-10Gd-2Y-1Al	9.62	2.09	1.00	bal.

III. RESULTS

A. *Grain Size*

The optical micrographs of one Mg-Gd-Y base alloy and two Mg-Gd-Y alloys with Al additions at different cooling rates were selected as examples to show the influence of cooling rate on grain size and morphology. Figure 1 shows the optical micrographs of Mg-5Gd-1Y alloys cooled at four rates in the range from 1.4 to 22.6 K/s. At the cooling rate of 1.4 and 3.0 K/s, the grains were columnar dendritic (Figures 1(a) and (b)). Increasing the cooling rate to 16.5 K/s led to a remarkable decrease in grain size, while the grain morphology remained dendritic (Figure 1(c)). The grain size and morphology changed slightly when the cooling rate was further increased to 22.6 K/s (Figure 1(d)).

Figure 2 shows the optical micrographs of Mg-5Gd-1Y alloys with 1 pct Al addition cooled at different rates. At the cooling rate of 1.4 and 3.0 K/s, the grains were equiaxed dendritic (Figures 2(a) and (b)) and were significantly refined compared to the Mg-5Gd-1Y base alloys cooled at the same rate (Figures 1(a) and (b)). However, the grains became coarsened when the cooling rate was increased to 16.5 and 22.6 K/s (Figures 2(c) and (d)), contrary to general observations that grains become refined with increasing cooling rate.[7,13,14]

The optical micrographs of Mg-10Gd-2Y alloys with 1 pct Al addition are shown in Figure 3. The grains were

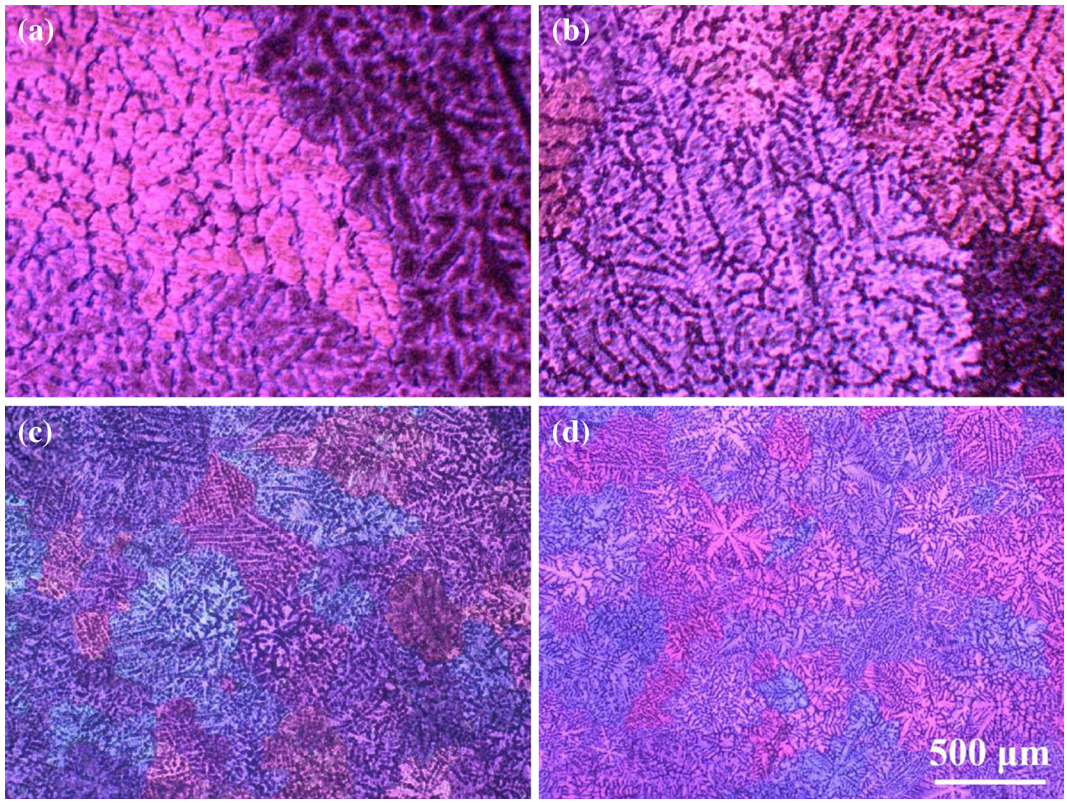

Fig. 1—Optical micrographs of Mg-5Gd-1Y alloy cooled at four rates: (*a*) 1.4 K/s, (*b*) 3.0 K/s, (*c*) 16.5 K/s, and (*d*) 22.6 K/s.

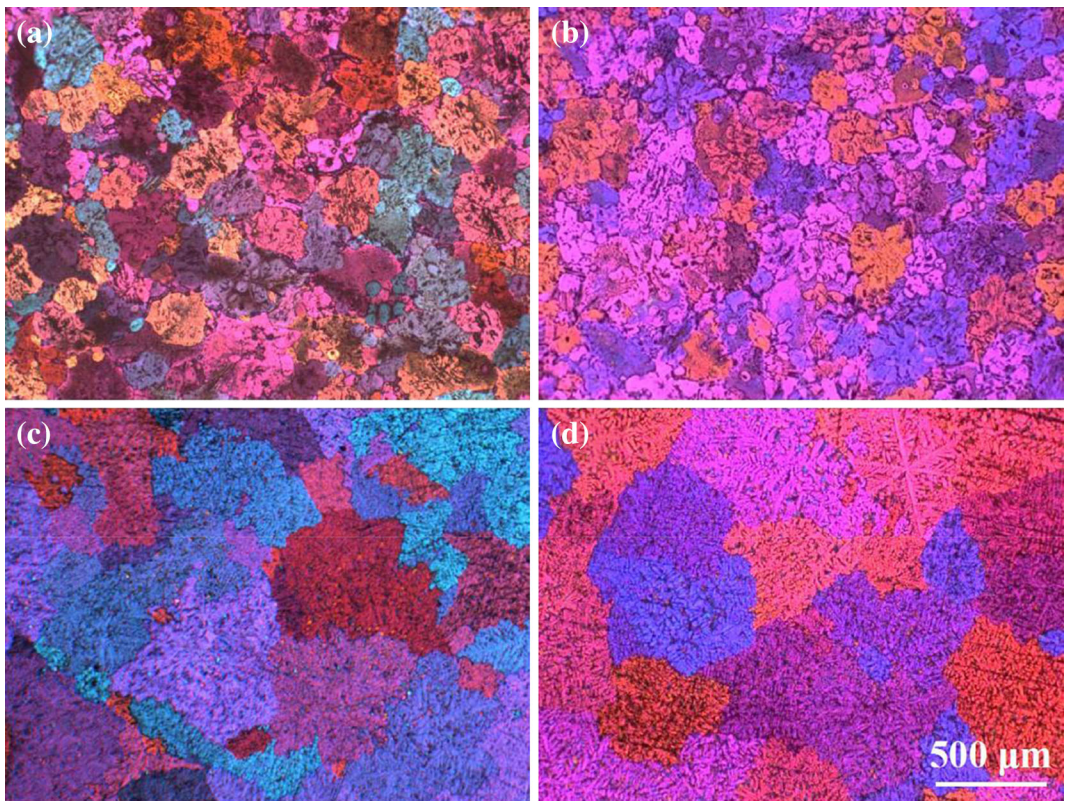

Fig. 2—Optical micrographs of Mg-5Gd-1Y-1Al alloy cooled at four rates: (*a*) 1.4 K/s, (*b*) 3.0 K/s, (*c*) 16.5 K/s, and (*d*) 22.6 K/s.

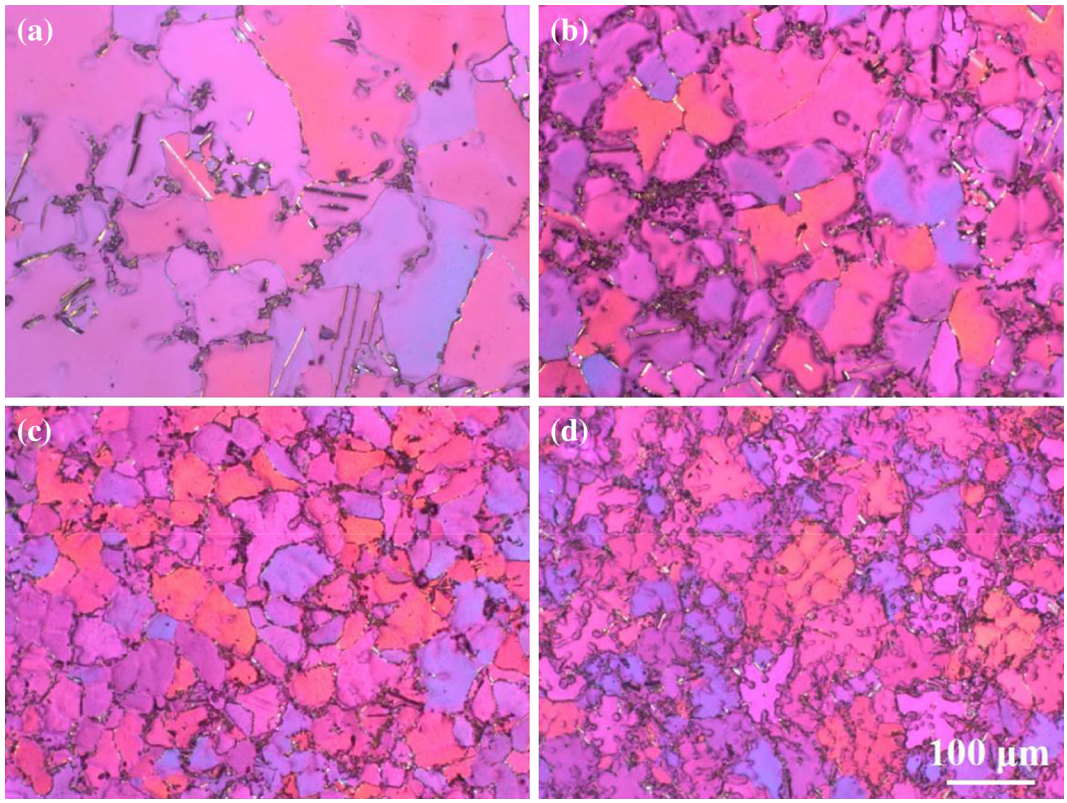

Fig. 3—Optical micrographs of Mg-10Gd-2Y-1Al alloy cooled at four rates: (*a*) 1.4 K/s, (*b*) 3.0 K/s, (*c*) 16.5 K/s, and (*d*) 22.6 K/s.

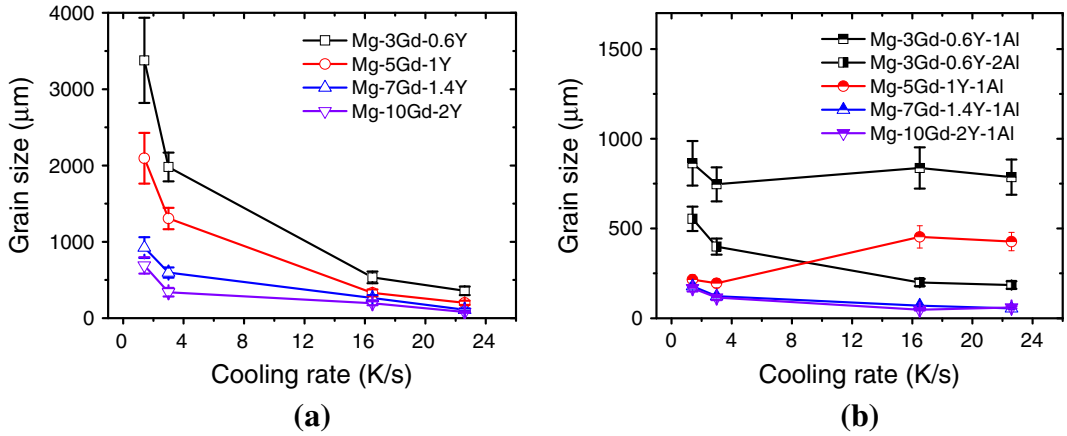

Fig. 4—Variation in grain sizes of (*a*) Mg-Gd-Y base alloys and (*b*) Mg-Gd-Y alloys with Al additions as a function of cooling rate.

equiaxed with an irregular shape at a cooling rate of 1.4 K/s (Figure 3(a)). Increasing the cooling rate to 3.0 K/s led to grain refinement and a rosette-like morphology (Figure 3(b)). The grains were further refined, and the grain morphology became slightly more dendritic when the cooling rate was further increased to 16.5 K/s (Figure 3(c)). At a cooling rate of 22.6 K/s, the grain size showed a slight change but the grain morphology became more dendritic (Figure 3(d)). The present grain morphology became more dendritic with increasing cooling rate, which is similar to that of Al alloys.[28,29]

Figure 4(a) shows the variation of grain sizes of Mg-Gd-Y base alloys with cooling rate. Grain sizes of all base alloys decreased with increasing cooling rate, particularly when the cooling rate was below 16.5 K/s. Furthermore, alloys with lower solute contents (Mg-3Gd-0.6Y and Mg-5Gd-1Y alloys) had a larger initial grain size but also showed a higher tendency to be grain refined by increasing the cooling rate than those with higher solute contents (Mg-7Gd-1.4Y and Mg-10Gd-2Y alloys). Figure 4(b) shows the variation of grain sizes of Al-refined Mg-Gd-Y alloys with cooling rate. Mg-3Gd-0.6Y-2Al, Mg-7Gd-1.4Y-1Al, and Mg-10Gd-2Y-1Al

alloys also generally showed a tendency to be grain refined with increasing cooling rate, while grains in Mg-3Gd-0.6Y-1Al and Mg-5Gd-1Y-1Al alloys became coarsened as the cooling rate was increased from 3.0 to 16.5 K/s. When the Al addition was 1 pct, the grain size generally decreased with increasing Gd and Y contents at each cooling rate.

B. *Microstructures of Mg-Gd-Y Alloys with Al Additions*

Microstructures of Mg-Gd-Y base alloys have been described previously and consist of dendritic primary α-Mg and irregular-shaped Mg-Gd-Y intermetallic particles distributed in the dendritic regions or grain boundaries.[30,31] In the present paper, the microstructures of alloys with Al additions were examined to investigate the grain refining/coarsening mechanism.

Figure 5 shows the backscattered electron (BSE) images of Mg-10Gd-2Y-1Al samples cooled at different rates. Four types of intermetallic particles were observed: polygonal (labeled as "P1"-"P4"), irregular-shaped (labeled as "I"), petal-like (labeled as "L1" and "L2"), and plate-shaped particles (labeled as "S1" and "S2"). The polygonal, irregular-shaped, and petal-like particles were also observed in the Mg-10Gd-3Y-0.8Al alloy cast into a steel mold.[24] Table II shows the EDX results from these particles. The polygonal particles mainly consist of Al and (Gd + Y) with atomic ratio of Al:(Gd + Y) close to 2:1, suggesting that these polygonal particles are $Al_2(Gd_xY_{1-x})$.[24] The irregular-shaped particle (labeled as "I") consisting of Mg, Gd, Y, and a small amount of Al appears to be $Mg_{24}(Gd, Y)_5$ with trace Al dissolved.[24,32] The petal-like particles (labeled as "L1" and "L2") containing Gd, Y, and Al with a balance of Mg might be $(Mg, Al)_3(Gd_xY_{1-x})$.[24] The plate-shaped particles (labeled as "S1" and "S2") with similar compositions to the petal-like particles might also be $(Mg, Al)_3(Gd_xY_{1-x})$. All particle morphologies were refined with increasing cooling rate, particularly from 3.0 to 16.5 K/s, where the plate-shaped particles appeared to transform into petal-like particles.

Microstructures of the other alloys with Al additions were also examined. Similar to the microstructure in the Mg-10Gd-2Y-1Al alloy, $Al_2(Gd_xY_{1-x})$ polygonal particles were formed and the particle morphology was refined with increasing cooling rate. In most alloys, such as Mg-10Gd-2Y-1Al (Figure 5) and Mg-3Gd-0.6Y-2Al (Figure 6), the polygonal $Al_2(Gd_xY_{1-x})$ particles were reproducibly observed at grain centers and they are likely to have acted as heterogeneous nucleation sites for α-Mg.[24] In contrast, in the Mg-5Gd-1Y-1Al alloy, while polygonal particles were found at grain centers when the cooling rate was 1.4, 3.0, and 16.5 K/s (Figures 7(a) through (d)), with the cooling rate increased from 3.0 to 16.5 K/s, the number density of these particles at grain centers was remarkably decreased and they were rarely observed. No $Al_2(Gd_xY_{1-x})$ particles were observed at grain centers at the cooling rate of 22.6 K/s (Figures 7(e) and (f)), which might be due to the scarcity of these particles. In the Mg-3Gd-0.6Y-1Al alloy, few $Al_2(Gd_xY_{1-x})$ polygonal particles were observed at grain centers at cooling rates of 1.4 and 3.0 K/s, and no particles were found at grain centers with increasing the cooling rate to 16.5 and 22.6 K/s. The remarkable decrease or disappearance of active $Al_2(Gd_xY_{1-x})$ nucleants appears to account for the grain coarsening rather than refining in both Mg-5Gd-1Y-1Al and Mg-3Gd-0.6Y-1Al alloys with the cooling rate increased from 3.0 to 16.5 K/s (Figure 4(b)).

C. *Size Distribution and Number Density and of $Al_2(Gd_xY_{1-x})$ Particles*

Figures 5, 6, and 7 indicate that solute concentration and cooling rate remarkably affect the number density and morphology of intermetallic particles including $Al_2(Gd_xY_{1-x})$ nucleant particles. Because the number density[33] and size[5] of nucleant particles significantly influence grain refinement, the size distribution of total $Al_2(Gd_xY_{1-x})$ particles and of possible active $Al_2(Gd_xY_{1-x})$ particles in the Al-refined Mg-Gd-Y alloys cooled at different rates was measured as shown in Figure 8 (the $Al_2(Gd_xY_{1-x})$ particles in Mg-5Gd-1Y-1Al samples cooled at 16.5 and 22.6 K/s and in Mg-3Gd-0.6Y-1Al samples are too few to measure the size distribution). It should be noted that in Figure 8 each point in the size range from 0 to 10 μm and from 10 to 35 μm represents the relative frequency of particles within the size range of ±0.5 and ±2.5 μm, respectively. In each alloy, the particle size distribution was similar at cooling rates of 1.4 and 3.0 K/s, and at cooling rates of 16.5 and 22.6 K/s, the particle size distribution was also similar. At slow cooling rates (1.4 and 3.0 K/s), the particle size distribution spanned a larger range and the relative frequency of large particles was generally higher than that at high cooling rates (16.5 and 22.6 K/s).

It has been found that the majority of active nucleants are larger than a certain value which varies in different systems.[7,34,35] This phenomenon was also observed in the current investigations. As can be seen in Figure 8, a critical size d_p can be invariably defined, where ~90 pct active nucleation particles are larger than d_p. The statistics of d_p in all alloys at different cooling rates are shown in Table III. The area number density (ρ_{ns}) of $Al_2(Gd_xY_{1-x})$ particles larger than d_p is shown in Figure 9. ρ_{ns} is the number density of all $Al_2(Gd_xY_{1-x})$ nucleant particles that can be activated by the undercooling. ρ_{ns} in the Mg-3Gd-0.6Y-2Al alloy is generally lower than that in the 1 pct Al containing alloys (except for that in Mg-5Gd-1Y-1Al cooled at 16.5 and 22.6 K/s), which might be due to the high relative frequency of large particles and large d_p in the Mg-3Gd-0.6Y-2Al alloy as shown in Figure 8 and Table III.

IV. DISCUSSION

It has been found that the grain size of the as-cast samples is controlled by several factors, *i.e.*, nucleant substrates (number density, size, and potency of nucleation), solute,

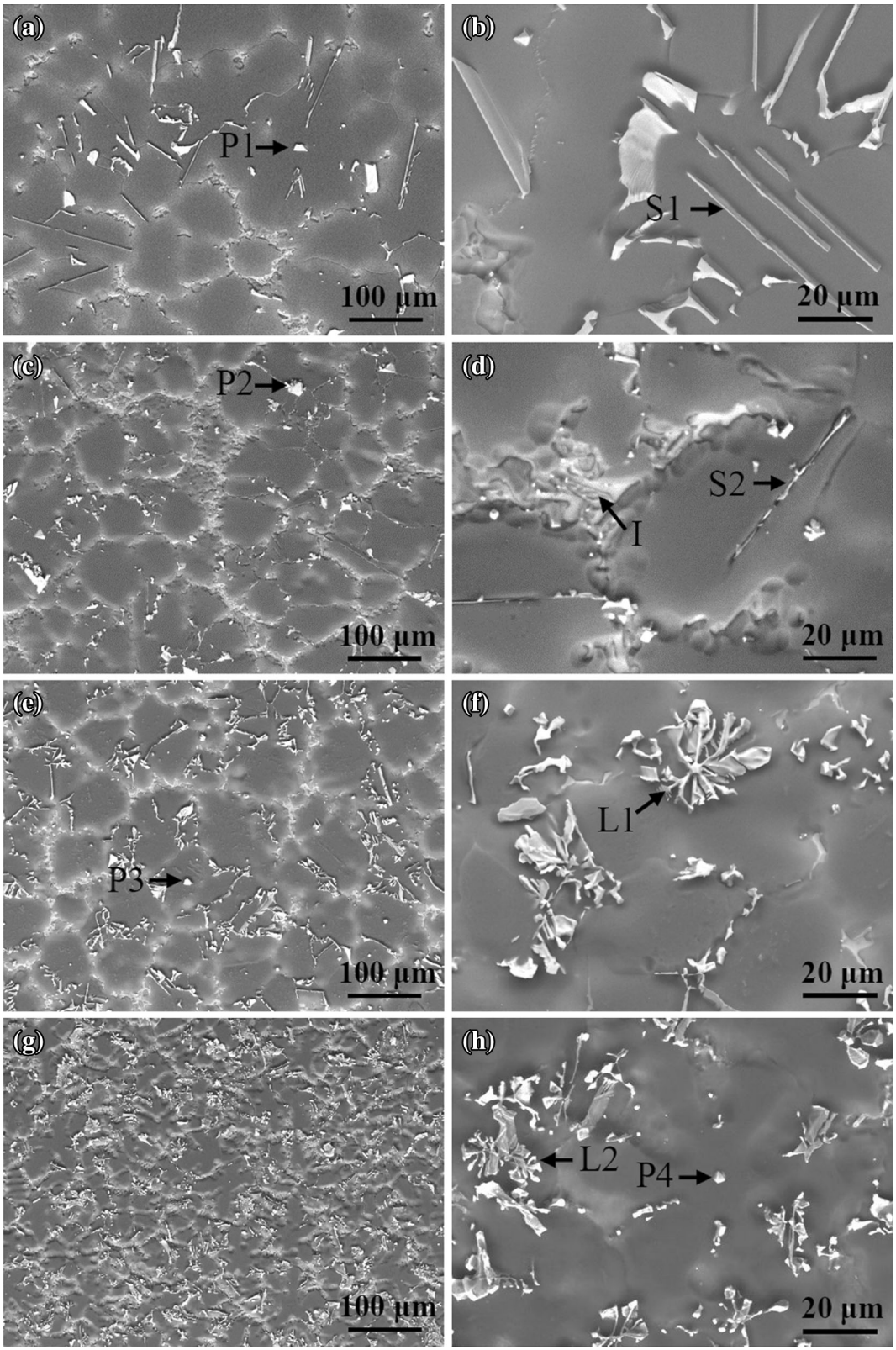

Fig. 5—SEM BSE images of Mg-10Gd-2Y-1Al alloy cooled at four rates: (*a*) and (*b*) 1.4 K/s, (*c*) and (*d*) 3.0 K/s, (*e*) and (*f*) 16.5 K/s and (*g*) and (*h*) 22.6 K/s. "P1"-"P4" denote polygonal particles; "S1" and "S2" denote plate-shaped particles; "I" denotes the irregular-shaped particle; and "L1" and "L2" denote petal-like particles.

and cooling conditions.[1,2,11] Considerable attempts have been dedicated to develop a model to correlate the grain sizes of cast samples with these parameters.[2,12,15,36] A similar approach will be used in the present work to understand the grain refining behavior of Mg-Gd-Y(-Al) alloys. The variation of $Al_2(Gd_xY_{1-x})$ nucleant particles in Mg-Gd-Y-Al alloys is discussed, and the grain refining behavior by Zr and Al additions is also compared.

A. *The Relationship Between Grain Size and Solute Content, Cooling Rate, and Number Density and Size of Nucleant Particles*

The growth restriction factor $Q = \sum_i m_i(k_i - 1)C_{0i}$ is a commonly accepted parameter to describe the effect of solute on grain size, where m is the gradient of the liquidus on the binary phase diagram, k is the solute partition coefficient, C_0 is the solute content, and i represents the ith solute element.[12] Grain sizes of Al base alloys were found to be proportional to the reciprocal of Q.[9,12] In a recent work, Easton and StJohn[2] found that when nucleant particles are known, the dependence of grain size on solute content, and the potency and number density of nucleant particles can be expressed:

$$d_{gs} = \frac{a}{\sqrt[3]{\rho_{nv}}} + \frac{b\Delta T_n}{Q} \quad [1]$$

where d_{gs} is the grain size, ρ_{nv} is the volume number density of nucleant particles in the melt, *i.e.*, the number of particles per unit volume, ΔT_n is the critical nucleation undercooling, and a and b are constants. The above relationship has also been applied to Mg alloys.[33]

The free growth theory proposes that when nucleants are potent, nucleation itself is not the controlling factor in grain initiation. Instead, the onset of free growth of a nucleus on a potent nucleant particle is the dominant factor, and the critical undercooling for free growth to occur, ΔT_{fg}, which reflects the barrier to free growth, is inversely proportional to the nucleant size, d_p[5,7,8]:

$$\Delta T_{fg} = \frac{4\sigma}{\Delta S_V d_p} \quad [2]$$

Table II. EDX Results of the Labeled Particles in Fig. 5

	Elemental Composition (at. pct)			
Particle	Mg	Al	Gd	Y
P1	8.3	60.5	22.5	8.7
P2	9.9	56.9	21.3	11.9
P3	6.9	61.4	24.5	7.2
P4	24.8	49.4	16.7	9.0
I	89.9	0.54	7.36	2.21
L1	61.9	18.4	14.7	5.0
L2	59.9	19.7	16.1	4.3
S1	65.5	15.8	15.2	3.5
S2	63.7	21.3	10.2	4.8

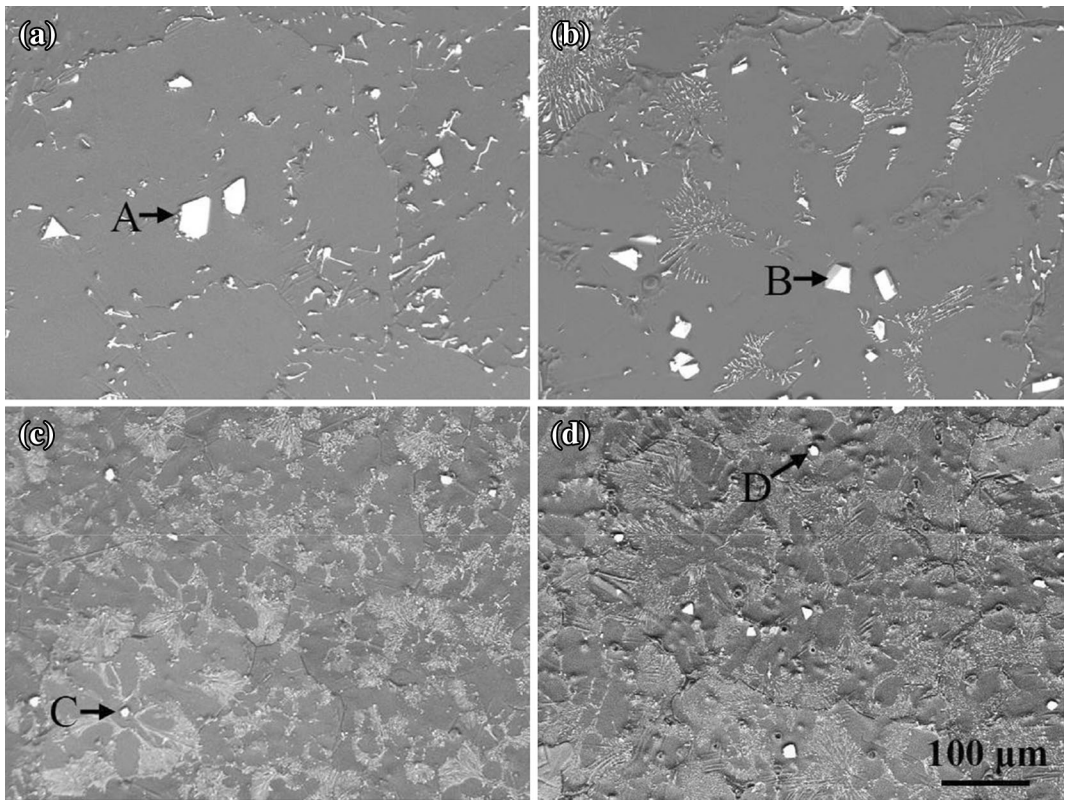

Fig. 6—SEM BSE images of Mg-3Gd-0.6Y-2Al alloy cooled at four rates: (*a*) 1.4 K/s, (*b*) 3.0 K/s, (*c*) 16.5 K/s and (*d*) 22.6 K/s. The particles labeled as "A", "B", "C", and "D" are $Al_2(Gd_xY_{1-x})$ polygonal particles.

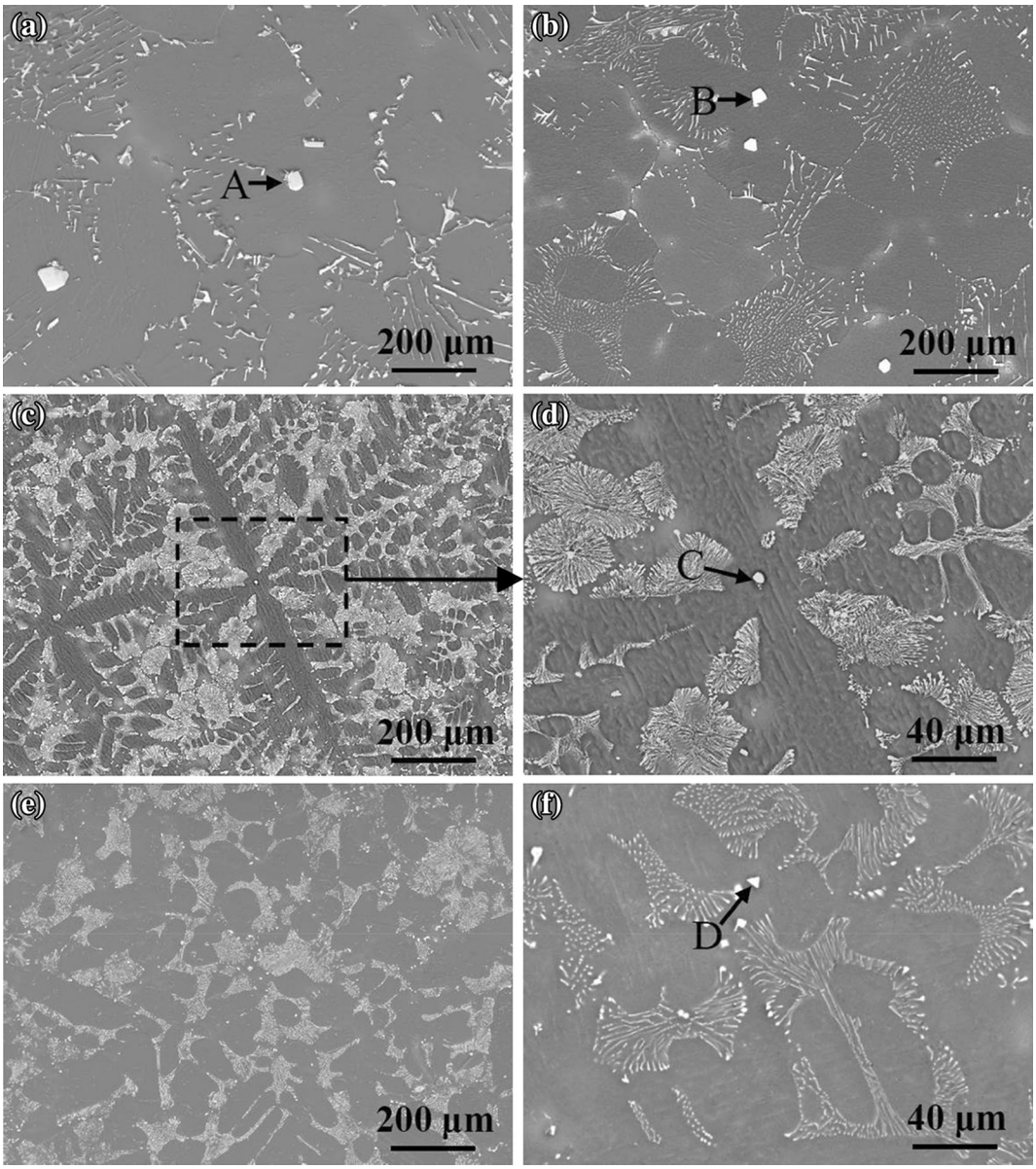

Fig. 7—SEM BSE images of Mg-5Gd-1Y-1Al alloy cooled at four rates: (*a*) 1.4 K/s, (*b*) 3.0 K/s, (*c*) and (*d*) 16.5 K/s and (*e*) and (*f*) 22.6 K/s. The particles labeled as "A", "B", "C", and "D" are $Al_2(Gd_xY_{1-x})$ polygonal particles.

where σ is the solid–liquid interfacial energy, and ΔS_V is the entropy of fusion per unit volume. As $Al_2(Gd_xY_{1-x})$ particles are potent nucleants for the Mg matrix,[24] ΔT_{fg} is considered to be dominant in grain initiation in Mg-Gd-Y-Al alloys. By replacing ΔT_n in Eq. [1] by ΔT_{fg} and substituting Eqs. [2] into [1], the grain size can be expressed as

$$d_{gs} = \frac{a}{\sqrt[3]{\rho_{nv}}} + \frac{4b\sigma}{\Delta S_V Q d_p} \quad [3]$$

In Eq. [3], σ and ΔS_V are constants, $\frac{4b\sigma}{\Delta S_V}$ is thus a constant. By defining $b_1 = \frac{4b\sigma}{\Delta S_V}$, Eq. [3] would be rewritten as

$$d_{gs} = \frac{a}{\sqrt[3]{\rho_{nv}}} + \frac{b_1}{Q d_p} \quad [4]$$

It should be noted that ρ_{nv} in the above equations is the volume number density. In the present work, the obtained ρ_{ns} is the area number density. ρ_{ns} can be converted to ρ_{nv} by the simple relationship: $\rho_{nv} = (\sqrt{\rho_{ns}})^3$,[37] thus Eq. [4] would be expected to be

$$d_{gs} = \frac{a_1}{\sqrt{\rho_{ns}}} + \frac{b_1}{Q d_p} \quad [5]$$

where a_1 is a constant.

In terms of the effect of cooling rate ($\dot{T}$) on grain size of cast samples, Johnsson found that the grain size is proportional to the reciprocal of square root of cooling rate, $\frac{1}{\sqrt{\dot{T}}}$.[25] Chai *et al.*[12] found that with both solute content and cooling rate considered, the grain size of Al alloys is proportional to $\frac{1}{Q\sqrt{\dot{T}}}$. Moreover, Easton and

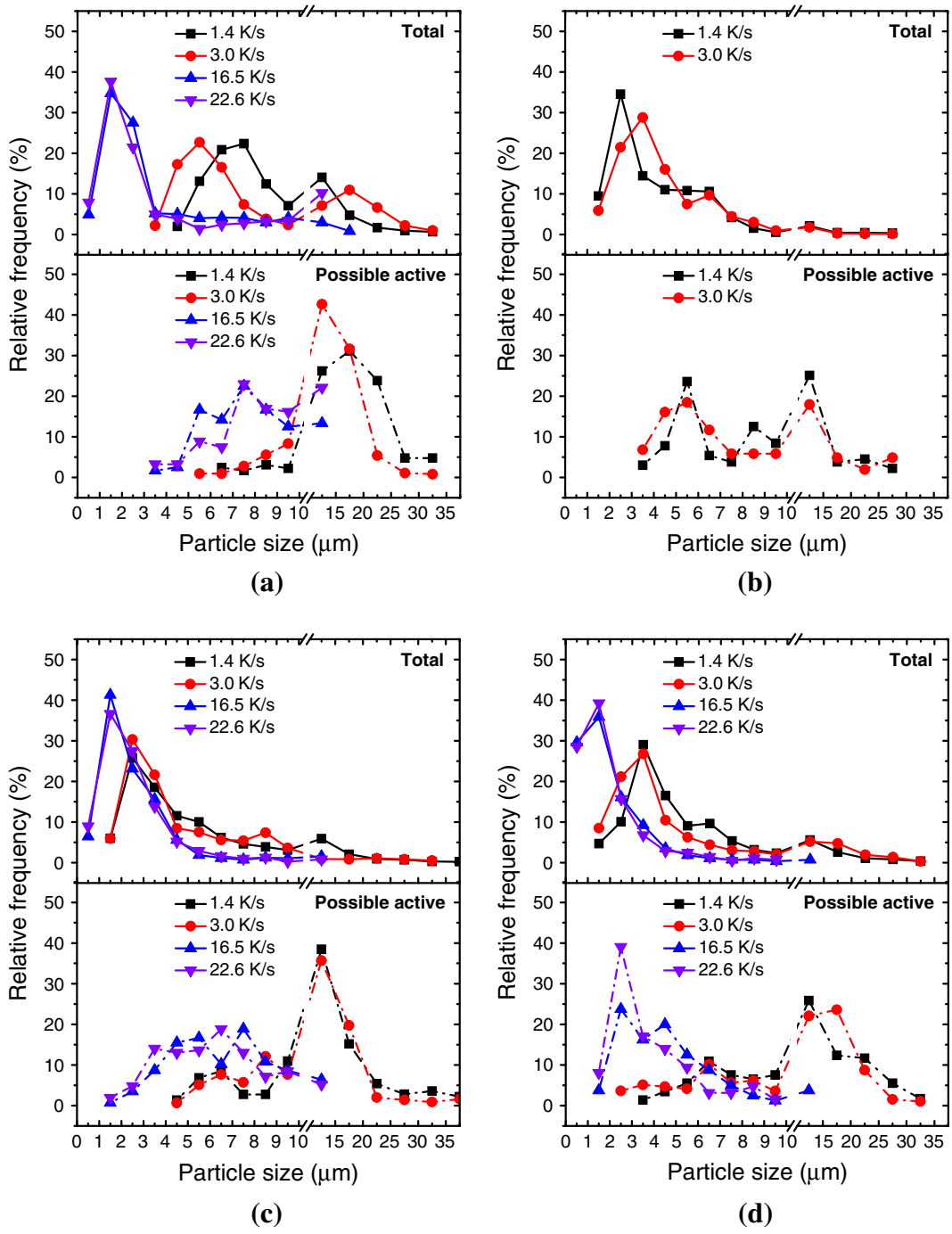

Fig. 8—Size distribution of total $Al_2(Gd_xY_{1-x})$ particles (the upper half of figures labeled as "Total") and of possible active $Al_2(Gd_xY_{1-x})$ particles (the lower half of figures labeled as "Possible active") in (*a*) Mg-3Gd-0.6Y-2Al, (*b*) Mg-5Gd-1Y-1Al, (*c*) Mg-7Gd-1.4Y-1Al, and (*d*) Mg-10Gd-2Y-1Al alloys cooled at different rates.

StJohn[15] found that with the presence of active nucleants, grain sizes are also linearly related to $\frac{1}{Q\sqrt{\dot{T}}}$:

$$d_{gs} = \frac{a}{\sqrt[3]{\rho_{nv}}} + \frac{b_2 \Delta T_n}{Q\sqrt{\dot{T}}} \quad [6]$$

where b_2 is a constant. Equation [6] is a detailed form of Eq. [1] with the cooling rate considered. Similarly, in the present work, when the cooling rate is considered, grain sizes of Mg-Gd-Y-Al alloys would be expected to be as follows:

$$d_{gs} = \frac{a_2}{\sqrt{\rho_{ns}}} + \frac{b_3}{Qd_p\sqrt{\dot{T}}} \quad [7]$$

where a_2 and b_3 are constants. Equation [7] is the format of Eq. [5] with the cooling rate considered.

Table III. Critical Size (d_p) of $Al_2(Gd_xY_{1-x})$ Particles to be Activated by the Constitutional Supercooling in Mg-Gd-Y-Al Alloys Cooled at Different Rates

Alloy	Cooling Rate (K/s)	d_p (μm)
Mg-3Gd-0.0.6Y-2Al	1.4	10
	3.0	9
	16.5	5
	22.6	5
Mg-5Gd-1Y-1Al	1.4	5
	3.0	4
	16.5	—
	22.6	—
Mg-7Gd-1.4Y-1Al	1.4	6
	3.0	6
	16.5	3
	22.6	3
Mg-10Gd-2Y-1Al	1.4	6
	3.0	6
	16.5	2
	22.6	2

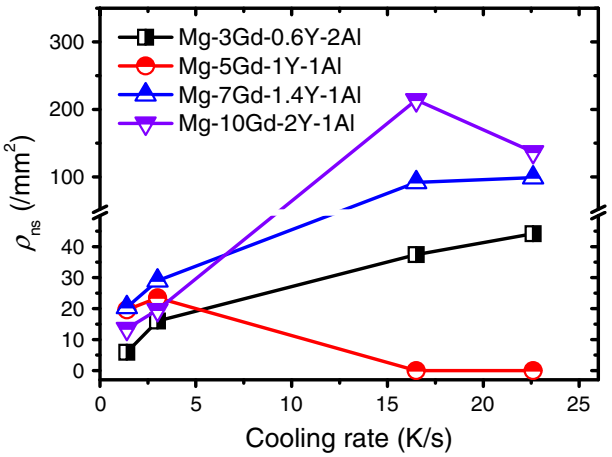

Fig. 9—Variation in area number density (ρ_{ns}) of $Al_2(Gd_xY_{1-x})$ nucleant particles larger than d_p in Mg-Gd-Y-Al alloys as a function of cooling rate.

The grain refining behavior of Al-free Mg-Gd-Y alloys and of Al containing Mg-Gd-Y-Al alloys is analyzed using the above equations as shown below.

1. *Al-free alloys*

For Mg-Gd-Y base alloys, no nucleant particles were inoculated by design. In this case, the heterogeneous nucleation is supposed to occur on certain "native nucleants"[36] available in the melt, while the size of these nucleants is independent on the solute concentration and cooling rate. Thus grain sizes of these alloys might be dominated by Q and $\dot{T}$. Table IV shows the m, k and $m(k-1)$ values for Gd and Y elements in Mg.[11,38] Figure 10 plots d_{gs} against $\frac{1}{Q}$, $\frac{1}{\sqrt{\dot{T}}}$ and $\frac{1}{Q\sqrt{\dot{T}}}$ for Mg-Gd-Y base alloys. In Figure 10(a), where the d_{gs} is plotted against $\frac{1}{Q}$, good linear relationships are observed (the values of correlation coefficient (R^2) are not less than 0.95 as shown in Table V). However, the values of

Table IV. Gradient of the Liquidus Line (m), Equilibrium Partition Coefficient (k), and $m(k-1)$, of Gd and Y in Mg[33,36]

Solute in Mg	m (K/Wt Pct)	k	$m(k-1)$ (K/Wt Pct)
Gd[36]	−2.66	0.61	1.04
Y[33]	−3.40	0.50	1.70

intercepts for the lines of best fit are below zero or negligible (Table V). Such small or even negligible intercept has also been observed in other Mg alloys.[11,39,40] The reason might be that the number density of "native nucleants" increases with solute content (although the identity of such nucleants is yet unknown[36]), which would skew the lines of best fit to be steeper than what should be and reduce the values of intercepts.[11,40]

The values of intercepts and gradients for the lines of best fit in Figure 10(b) where the d_{gs} is plotted against $\frac{1}{\sqrt{\dot{T}}}$ are shown in Table VI. The high R^2 values (not less than 0.91) indicate strong correlation between d_{gs} and $\frac{1}{\sqrt{\dot{T}}}$. The values of intercepts are below zero and also negligible (Table VI), which are considered to be within the experimental error.

In Figure 10(c), grain sizes of all base alloys are plotted against $\frac{1}{Q\sqrt{\dot{T}}}$. The high R^2 value (0.98) for the line of best fit suggests that d_{gs} is proportional to $\frac{1}{Q\sqrt{\dot{T}}}$. This implies that the gradient for lines of best fit would decrease with increasing Q or $\dot{T}$, which accounts for the decrease of gradient with increasing $\dot{T}$ and solute content in Figures 10(a) and (b), respectively. The reason that the intercept for the line of best fit in Figure 10(c) is negative might be the same as that why the intercepts in Figure 10(a) are negative or negligible.

2. *Al containing alloys*

For Mg-Gd-Y-Al alloys, nucleant particles are $Al_2(Gd_xY_{1-x})$ and their number density and size distribution are measurable, thus the dependence of grain sizes in these alloys not only on Q and $\dot{T}$, but also on ρ_{ns} and d_p can be studied.

It is worth noting that in the Al-refined alloys, the properitectic $Al_2(Gd_xY_{1-x})$ nucleant particles form prior to the solidification of α-Mg, which decreases the Al, Gd, and Y contents in the melt when α-Mg starts to form.[41] As the rare earth contents in Mg-7Gd-1.4Y-1Al and Mg-10Gd-xAl alloys in an early publication are close and the properitectic Al_2Gd and $Al_2(Gd_xY_{1-x})$ particles are isomorphic,[23,24] the solute Al concentration in the melt when α-Mg starts to form in the above two alloys is regarded to be similar. In the Mg-10Gd-xAl alloys, the majority of Al_2Gd particles started to form when Al concentration exceeds 0.65 pct.[23] By assuming that all of the excess Al above 0.65 pct are combined with Gd and Y to form $Al_2(Gd_xY_{1-x})$, the solute Al in the melt prior to the solidification of α-Mg is ~0.65 pct. Similarly, the rare earth contents in Mg-10Gd-2Y-1Al and Mg-10Gd-3Y-xAl

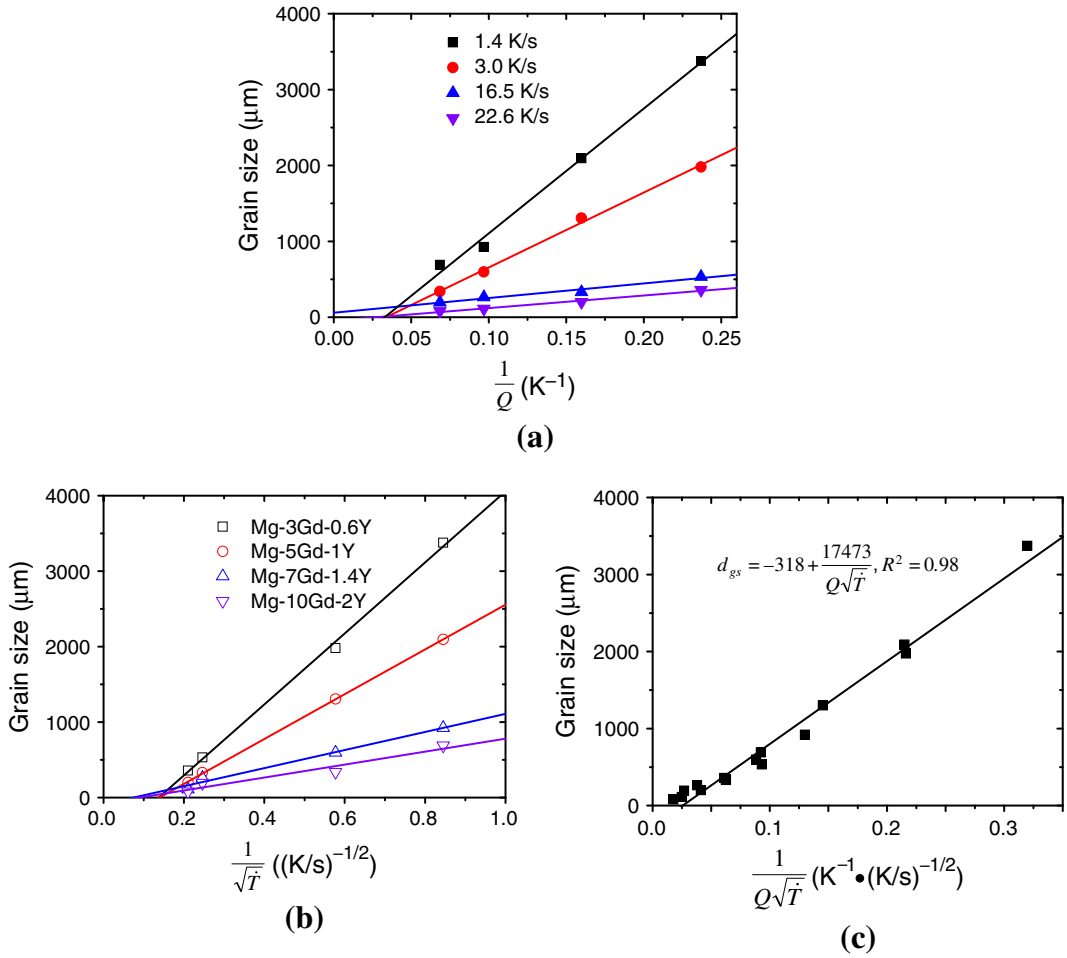

Fig. 10—Grain sizes of Mg-Gd-Y alloys plotted against (*a*) the reciprocal of growth restriction factor, $\frac{1}{Q}$, (*b*) the reciprocal of square root of cooling rate, $\frac{1}{\sqrt{\dot{T}}}$ and (*c*) $\frac{1}{Q\sqrt{\dot{T}}}$. Intercepts and gradients of the lines of best fit, and values of correlation coefficient (R^2) of the lines of best fit compared with the data they model in (a) and (b) are shown in Tables V and VI, respectively.

alloys in another early publication[24] are also close, thus the solute Al in the melt prior to the solidification of Mg is around 0.5 pct. The size distribution and number density of $Al_2(Gd_xY_{1-x})$ nucleant particles in Mg-5Gd-1Y-1Al and Mg-10Gd-2Y-1Al alloys are similar at the cooling rate of 3.0 K/s as shown in Figures 8 and 9 (the reason appears to be that the actual Al content in Mg-5Gd-1Y-1Al alloy is higher than that in Mg-10Gd-2Y-1Al alloy as shown in Table I), thus the amount of Al forming $Al_2(Gd_xY_{1-x})$ in the Mg-5Gd-1Y-Al alloy is considered to be approximately 0.5 pct. In $Al_2(Gd_xY_{1-x})$ particles, the x value is around 0.7 according to the results of EDX analysis shown in Table II. In the Mg-3Gd-0.6Y-1Al alloy, few $Al_2(Gd_xY_{1-x})$ particles were formed. Hence the amount of solute in the melt prior to the solidification of α-Mg in the Mg-3Gd-0.6Y-2Al alloy is estimated by assuming that the excess Al above 1 pct is combined with Gd and Y to form $Al_2(Gd_xY_{1-x})$ until nearly all the Y/Gd is used to form $Al_2(Gd_xY_{1-x})$ particles (solute concentrations in Mg-3Gd-0.6Y-2Al alloy are hard to estimate, and the value is of little reference and importance, because the data for this alloy are not used to relate the d_{gs} to Q, $\dot{T}$, ρ_{ns}, and d_p using Eqs. [5] or [7] as shown below). Based upon the above analysis, the estimated solutes Gd, Y, and Al in the melt not forming $Al_2(Gd_xY_{1-x})$ particles are shown in Table VII and these data are used to calculate Q-values accordingly.

In order to analyze the effect of solute content on grain size, the relationship between d_{gs}, $\frac{1}{\sqrt{\rho_{ns}}}$, and $\frac{1}{d_p Q}$ is fitted using Eq. [5]. Values of coefficients a_1 and b_1 are shown in Table VIII. The high values of R^2 (0.93 and 0.99) indicate that the data fit well with Eq. [5]. The data for the Mg-3Gd-0.6Y-2Al alloy are not included during the above analysis, because the same Q value contributed by different elements is expected to correspond to different grain sizes.[11] The reason might be that different solutes in Mg have different liquids/solidus line's gradients, which would affect the undercooling in front of the solid–liquid interface and subsequent refined grain size.[42] Al is the main contributing factor to Q in the Mg-3Gd-0.6Y-2Al alloy, while Gd and Y are the main contributing factors to Q in the above three alloys. At cooling rates of 16.5 and 22.6 K/s, the number density of nucleant particles in Mg-5Gd-1Y-1Al samples was not able to be determined, and the amount of data is insufficient to fit the d_{gs} with $\frac{1}{\sqrt{\rho_{ns}}}$ and $\frac{1}{d_p Q}$.

Table V. Intercepts and Gradients of the Lines of Best Fit in Fig. 10(a), and Values of R^2 of the Lines of Best Fit Compared with the Data They Model

Cooling Rate (K/s)	Intercept (μm)	Gradient (μm K)	R^2
1.4	−540	16,452	0.99
3.0	−332	9880	0.95
16.5	59	1930	0.98
22.6	−45	1656	0.99

Table VI. Intercepts and Gradients of the Lines of Best Fit in Fig. 10(b), and Values of R^2 of the Lines of Best Fit Compared with the Data They Model

Alloy	Intercept (μm)	Gradient (μm (K/s)$^{1/2}$)	R^2
Mg-3Gd-0.6Y	−646	4702	0.99
Mg-5Gd-1Y	−412	2969	0.99
Mg-7Gd-1.4Y	−89	1200	0.98
Mg-10Gd-2Y	−77	858	0.91

Table VII. Predicted Contents of Gd, Y and Al Elements Left in the Melt Prior to the Solidification of α-Mg in Mg-Gd-Y-Al Alloys

	Elemental Composition (Wt Pct)		
Alloy	Al	Gd	Y
Mg-3Gd-0.6Y-2Al*	1.43	0.66	0.10
Mg-5Gd-1Y-1Al	0.80	3.39	0.38
Mg-7Gd-1.4Y-1Al	0.65	5.94	0.84
Mg-10Gd-2Y-1Al	0.5	8.60	1.84

Note: the solute contents in Mg-3Gd-0.6Y-2Al alloy is hard to estimate, and the value is of little reference and importance, because the data for this alloy is not used to relate the d_{gs} to Q, $\dot{T}$, ρ_{ns} and d_p using Eqs. [5] or [7].

Table VIII. Values of Coefficients a_1 and b_1 for Fitting the Grain Size of Mg-Gd-Y-Al Alloys with $\frac{1}{\sqrt{\rho_{ns}}}$ and $\frac{1}{d_p Q}$ Using Eq. [5], and Values of R^2 of the Lines of Best Fit Compared with the Data They Model

Cooling Rate (K/s)	a (10^{-3})	b_1 (μm^2 (K/s)$^{1/2}$)	R^2
1.4	364	5950	0.93
3.0	300	4061	0.99
16.5	—	—	—
22.6	—	—	—

According to Eq. [7], for a particular alloy composition, where the Q value is fixed, the d_{gs} would be related to ρ_{ns}, d_p, and $\dot{T}$:

$$d_{gs} = \frac{a_2}{\sqrt{\rho_{ns}}} + \frac{b_4}{d_p\sqrt{\dot{T}}} \quad [8]$$

where b_4 is a constant. By fitting the d_{gs} with $\frac{1}{\sqrt{\rho_{ns}}}$ and $\frac{1}{d_p\sqrt{\dot{T}}}$ using Eq. [8], values of coefficients a_2 and b_4 for each alloy are shown in Table IX. R^2 values not less than 0.93 indicate excellent fits with Eq. [8]. The amount of data for the Mg-5Gd-1Y-1Al samples is insufficient to relate the d_{gs} to $\frac{1}{\sqrt{\rho_{ns}}}$ and $\frac{1}{d_p\sqrt{\dot{T}}}$.

Table IX. Values of Coefficients a_2 and b_4 for Fitting the d_{gs} of each Mg-Gd-Y-Al Alloy with $\frac{1}{\sqrt{\rho_{ns}}}$ and $\frac{1}{d_p\sqrt{\dot{T}}}$ using Eq. [8], and Values of R^2 of the Lines of Best Fit Compared with the Data They Model

Alloy	a (10^{-3})	b_4 (μm^2 (K/s)$^{1/2}$)	R^2
Mg-3Gd-0.6Y-2Al	1300	113	0.93
Mg-5Gd-1Y-1Al	—	—	—
Mg-7Gd-1.4Y-1Al	721	17	0.97
Mg-10Gd-2Y-1Al	505	129	0.96

When all factors affecting the grain size are considered, grain sizes of Mg-Gd-Y-Al alloys can be related to $\frac{1}{\sqrt{\rho_{ns}}}$ and $\frac{1}{Qd_p\sqrt{\dot{T}}}$ by Eq. [7]. Data of Mg-5Gd-1Y-1Al, Mg-7Gd-1.4Y-1Al, and Mg-10Gd-2Y-1Al alloys were used to analyze the relationship. Values of coefficients a_2 and b_3 are 632 and 159, respectively. The R^2 value is 0.8, indicating the data fit with Eq. [7].

B. *Variation of Size Distribution of $Al_2(Gd_xY_{1-x})$ Particles with Cooling Rate and Size Distribution of Active Nucleants*

Figure 9 shows that the size of the polygonal $Al_2(Gd_xY_{1-x})$ particles in Mg-Gd-Y-Al alloys decreases with increasing cooling rate, which is similar to previous results that the morphology of intermetallic particles is refined with increasing cooling rate.[16,17,43,44] As their morphology changes with cooling rate, $Al_2(Gd_xY_{1-x})$ nucleant particles must form after the samples were taken from the crucible and prior to the solidification of α-Mg, *i.e.*, between 923 K and 1013 K (650 °C and 740 °C) similar to the pro-peritectic Al_2Y particles in Mg-Y-Al ternary alloys.[41] When the cooling rate increases, the time for $Al_2(Gd_xY_{1-x})$ particles to grow decreases during solidification, leading to smaller particles. The microstructure of the 1013 K (740 °C) Mg-10Gd-2Y-1Al melt quenched into water is shown in Figure 11 to check whether $Al_2(Gd_xY_{1-x})$ particles were formed in the crucible before samples were taken from the crucible. Few polygonal particles larger than 3 μm (marked by *arrow* in Figure 11) were observed, confirming that the nucleant particles were mainly formed during the cooling of the melt.

Similar to earlier observations,[7,8,23,34,35] the size of possible active nucleant particles in each sample is generally larger than a certain value (Table III), which can be explained by the free growth theory suggesting that ΔT_{fg} increases with decreasing size of nucleant particle.[7] Hence, nucleation first occurs on the largest particles, and further free growth on smaller particles is stifled by latent heat release[7] and/or the nucleation-free zone, where CS is smaller than the undercooling required for grains to nucleate and nucleation is suppressed.[36]

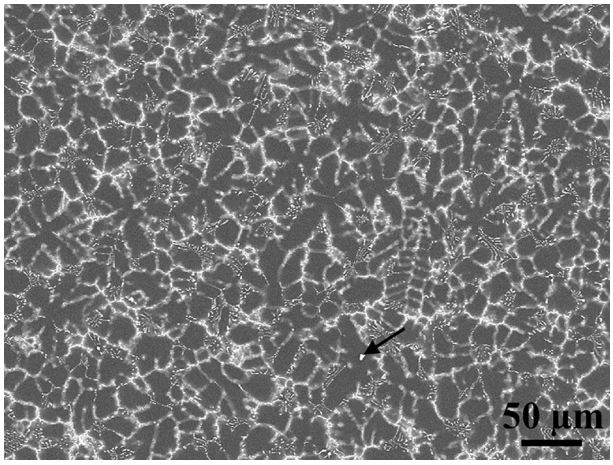

Fig. 11—SEM BSE image of the 1013 K (740 °C) Mg-10Gd-2Y-1Al melt quenched into water. The particle marked by arrow is an $Al_2(Gd_xY_{1-x})$ particle.

C. *Comparison with the Grain Refinement Effect of Zr*

Zr has, until now, been considered to be the most potent grain refiner for Al-free Mg alloys.[1,45] The excellent grain refining efficiency of Zr is attributed to both undissolved and dissolved Zr: the undissolved Zr particles act as potent heterogeneous nucleating substrates during solidification,[46] while the soluble Zr strongly restricts the growth of Mg grains and provides CS to promote nucleation.[11,47–49] Recently, Sun *et al.*[50] found that regardless of what kind of Mg-Zr master alloy was used, grain sizes of Mg-Gd-Y alloys with not less than 0.4 pct Zr additions cooled in air were always below 160 μm. When the cooling rate was reduced from 22.6 to 1.4 K/s, the grain size of Mg-10Gd-2Y alloy with 0.38 pct Zr introduced by the AM-CAST® master alloy (a Mg-25 pct Zr alloy)[51] increased from 48 to 85 μm.

Compared to the consistent fine grain size of the Zr-refined counterparts, the grain size of the Al-refined Mg-Gd-Y alloys is significantly influenced by Gd and Y contents and cooling rate (Figure 4(b)). One reason is that Gd and Y contents and cooling rate affect the number density and size distribution of nucleant particles (Figures 8 and 9) and consequently the subsequent nucleation of α-Mg, while the undissolved Zr particles acting as nucleation sites are independent on the Gd and Y contents and cooling rate when Zr is used to refined grains. Moreover, Gd and Y are also the main contributors to Q (rather than Zr) when the majority of Al reacts with Gd and Y to form $Al_2(Gd_xY_{1-x})$ prior to solidification of α-Mg. Hence, Gd and Y contents have a significant influence on the grain size (Figure 4(b)).

The grain size of the 1 pct Al-refined Mg-10Gd-2Y alloy cooled at 1.4 to 22.6 K/s varies in the range from 167 to 47 μm (Figure 4(b)), a much larger range than that of the 0.38 pct Zr-refined counterpart (85 to 48 μm). With decreasing cooling rate, d_p increases (Figure 8), which can decrease the refined grain size according to Eq. [7]. However, ρ_{ns} decreases with deceasing cooling rate (Figure 9), which would increase the final grain size. If d_p and ρ_{ns} remain unchanged (2 μm and 137/mm^2, respectively) when the cooling rate is reduced from 22.6 to 1.4 K/s, the grain size of the 1 pct Al-refined Mg-10Gd-2Y alloy cooled at 1.4 K/s would be 97 μm according to Eq. [8] and the values of coefficients shown in Table IX, much smaller than the actual grain size (167 μm). Hence, the decrease in ρ_{ns} dominates the variation of grain size and leads to an increase in the final grain size. To obtain a grain refining efficiency comparable to that of Zr, a fast cooling rate and high solute contents are needed when Al is used to refine grains of Mg-Gd-Y alloys.

V. CONCLUSIONS

1. The additions of Al to Mg-Gd-Y alloys generally lead to the formation of $Al_2(Gd_xY_{1-x})$ nucleant particles and consequent grain refinement.
2. The number density and size distribution of $Al_2(Gd_xY_{1-x})$ nucleant particles are affected by both solute content and cooling rate. The number density generally increases with both solute content and cooling rate, while the size of particles decreases significantly with increasing cooling rate from 3.0 to 16.5 K/s.
3. Grain sizes of Mg-Gd-Y base alloys are found to be $d_{gs} = a + \frac{b}{Q\sqrt{\dot{T}}}$, and grain sizes of Al-refined samples are found to be $d_{gs} = \frac{a'}{\sqrt{\rho_{ns}}} + \frac{b'}{\sqrt{\dot{T}Qd_p}}$, where a, b, a' and b' are constants.
4. Compared to the consistent fine grain size of the Zr-refined alloys, the grain size of the Al-refined Mg-Gd-Y alloys is significantly influenced by Gd and Y contents and cooling rate. When Al is used to refine grains of Mg-Gd-Y alloys, a high cooling rate and high solute contents are needed to obtain a good grain refining efficiency.

ACKNOWLEDGMENTS

The work is sponsored by the National Natural Science Foundation of China (No. 51275295), CAST Cooperative Research Centre of Australia, ARC Discovery Grant DP2010000071 (ME, DQ, MZ) and Research Fund for the Doctoral Program of Higher Education of China (Nos. 20120073120011 and 20130073110052). The authors acknowledge Monash Centre for Electron Microscopy (MCEM) for access to experimental facilities and thank Mr. Andrew Yob and Mrs. Maya Gershenzon at CSIRO for help with experiments.

REFERENCES

1. D.H. StJohn, M.A. Easton, M. Qian, and J.A. Taylor: *Metall. Mater. Trans. A*, 2013, vol. 44A, pp. 2935–49.
2. M. Easton and D. StJohn: *Metall. Mater. Trans. A*, 2005, vol. 36A, pp. 1911–20.

3. M. Easton and D. StJohn: *Metall. Mater. Trans. A*, 1999, vol. 30A, pp. 1613–23.
4. D. Turnbull: *Acta Metall.*, 1953, vol. 1, pp. 8–14.
5. A.L. Greer: *Philos. Trans. R. Soc. Lond. A*, 2003, vol. 361, pp. 479–95.
6. D. Turnbull: *J. Chem. Phys.*, 1950, vol. 18, pp. 198–203.
7. A.L. Greer, A.M. Bunn, A. Tronche, P.V. Evans, and D.J. Bristow: *Acta Mater.*, 2000, vol. 48, pp. 2823–35.
8. T.E. Quested and A.L. Greer: *Acta Mater.*, 2004, vol. 52, pp. 3859–68.
9. M. Easton and D. StJohn: *Metall. Mater. Trans. A*, 1999, vol. 30A, pp. 1625–33.
10. M.A. Easton and D.H. StJohn: *Acta Mater.*, 2001, vol. 49, pp. 1867–78.
11. D. StJohn, M. Qian, M. Easton, P. Cao, and Z. Hildebrand: *Metall. Mater. Trans. A*, 2005, vol. 36A, pp. 1669–79.
12. G. Chai, L. Backerud, and L. Arnberg: *Mater. Sci. Technol.*, 1995, vol. 11, pp. 1099–103.
13. D. Eskin, Q. Du, D. Ruvalcaba, and L. Katgerman: *Mater. Sci. Eng. A*, 2005, vol. 405, pp. 1–10.
14. X. Zeng, Y. Wang, W. Ding, A. Luo, and A. Sachdev: *Metall. Mater. Trans. A*, 2006, vol. 37A, pp. 1333–41.
15. M.A. Easton and D.H. StJohn: *Mater. Sci. Eng. A*, 2008, vol. 486, pp. 8–13.
16. Y. Lü, Q. Wang, X. Zeng, W. Ding, C. Zhai, and Y. Zhu: *Mater. Sci. Eng. A*, 2000, vol. 278, pp. 66–76.
17. J. Bai, Y. Sun, F. Xue, and J. Qiang: *Mater. Sci. Eng. A*, 2012, vol. 552, pp. 472–80.
18. E.F. Emley: *Principles of Magnesium Technology*, Pergamon Press, Oxford, 1966.
19. I.A. Anyanwu, S. Kamado, and Y. Kojima: *Mater. Trans.*, 2001, vol. 42, pp. 1212–18.
20. T. Honma, T. Ohkubo, K. Hono, and S. Kamado: *Mater. Sci. Eng. A*, 2005, vol. 395, pp. 301–06.
21. S.M. He, X.Q. Zeng, L.M. Peng, X. Gao, J.F. Nie, and W.J. Ding: *J. Alloy. Compd.*, 2006, vol. 421, pp. 309–13.
22. D. Qiu, M.X. Zhang, J.A. Taylor, and P.M. Kelly: *Acta Mater.*, 2009, vol. 57, pp. 3052–59.
23. J. Dai, M. Easton, S. Zhu, G. Wu, and W. Ding: *J. Mater. Res.*, 2012, vol. 27, pp. 2790–97.
24. J. Dai, S. Zhu, M.A. Easton, M. Zhang, D. Qiu, G. Wu, W. Liu, and W. Ding: *Mater. Sci. Eng. A*, 2013, vol. 576, pp. 298–305.
25. M. Johnsson: *Z. Metall.*, 1994, vol. 85, pp. 781–85.
26. S. Cashion, N. Ricketts, and R. Bailey: *Proceedings of the 6th International Conference Magnesium Alloys and Their Applications*, Wiley, 2004, pp. 995–1000.
27. L. Backerud, E. Krol, and J. Tamminen: *Solidification Characteristics of Aluminium Alloys*, vol. 1, Skanaluminium, Universitetsforlaget As, Oslo, 1986.
28. M. Easton, C. Davidson, and D. St John: *Metall. Mater. Trans. A*, 2010, vol. 41A, pp. 1528–38.
29. M. Easton, C. Davidson, and D. StJohn: *Mater. Trans.*, 2011, vol. 52, pp. 842–47.
30. Z.K. Peng, X.M. Zhang, J.M. Chen, Y. Xiao, and H. Jiang: *Mater. Sci. Technol.*, 2005, vol. 21, pp. 722–26.
31. M. Sun, G. Wu, J. Dai, W. Wang, and W. Ding: *J. Alloy. Compd.*, 2010, vol. 494, pp. 426–33.
32. L. Gao, R.S. Chen, and E.H. Han: *J. Mater. Sci.*, 2009, vol. 44, pp. 4443–54.
33. D.H. StJohn, P. Cao, M. Qian, and M.A. Easton: *Adv. Eng. Mater.*, 2007, vol. 9, pp. 739–46.
34. A. Tronche and A.L. Greer: *Philos. Mag. Lett.*, 2001, vol. 81, pp. 321–28.
35. D. Qiu and M.X. Zhang: *J. Alloy. Compd.*, 2009, vol. 488, pp. 260–64.
36. D.H. StJohn, M. Qian, M.A. Easton, and P. Cao: *Acta Mater.*, 2011, vol. 59, pp. 4907–21.
37. E.E. Underwood: *Quantitative Stereology*, Addison-Wesley, Reading, MA, 1970.
38. A.A. Nayeb-Hashemi and J.B. Clark: *Phase Diagrams of Binary Magnesium Alloys*, ASM International, Materials Park, OH, 1988.
39. P. Cao, M. Qian, and D.H. StJohn: *Scripta Mater.*, 2007, vol. 56, pp. 633–36.
40. M. Sun, M.A. Easton, D.H. Stjohn, G. Wu, T.B. Abbott, and W. Ding: *Adv. Eng. Mater.*, 2013, vol. 15, pp. 373–78.
41. H.W. Chang, D. Qiu, J.A. Taylor, M.A. Easton, and M.X. Zhang: *J. Magnes. Alloy.*, 2013, vol. 1, pp. 115–21.
42. D. Qiu and M.X. Zhang: *Mater. Sci. Forum*, 2010, vols. 654–656, pp. 671–74.
43. S.M. Zhu, B.L. Mordike, and J.F. Nie: *Mater. Sci. Eng. A*, 2008, vols. 483–484, pp. 583–86.
44. S. Pang, G. Wu, W. Liu, M. Sun, Y. Zhang, Z. Liu, and W. Ding: *Mater. Sci. Eng. A*, 2013, vol. 562, pp. 152–60.
45. M. Qian and D.H. Stjohn: *Int. J. Cast Met. Res.*, 2009, vol. 22, pp. 256–59.
46. P. Villars and L.D. Calvert: *Pearson's Handbook of Crystallographic Data for Intermetallic Phases*, 2nd ed., ASM International, Materials Park, OH, 1991.
47. M. Qian, D.H. StJohn, and M.T. Frost: *Mater. Sci. Forum*, 2003, vols. 419–422, pp. 593–98.
48. P. Cao, M. Qian, D.H. StJohn, and M.T. Frost: *Mater. Sci. Technol.*, 2004, vol. 20, pp. 585–92.
49. M. Qian: *Acta Mater.*, 2006, vol. 54, pp. 2241–52.
50. M. Sun, G. Wu, M. Easton, D. StJohn, T. Abbott, and W. Ding: *9th International Conference on Magnesium Alloys and their Applications*, 2012, pp. 873–80.
51. M. Qian, D.H. StJohn, and M.T. Frost: *Proceedings of the 6th International Conference Magnesium Alloys and Their Applications*, Wiley, New York, 2003, pp. 706–12.